Nonreciprocal coupled waveguides for integrated optical isolators and circulators for TM-modes

N. Bahlmann, M. Lohmeyer, A. Zhuromskii, H. Dötsch and P. Hertel
University of Osnabrück, 49069 Osnabrück, Germany

January 8, 1999

Abstract

Magneto-optic rib-waveguides can be utilized to construct the main component of devices like nonreciprocal Mach-Zehnder interferometers or nonreciprocal directional couplers. In this paper we present detailed investigations of nonreciprocal couplers formed by double layer rib-waveguides with alternating sign of the Faraday rotation. The performance of the proposed devices is simulated by normal mode theory and simple beam propagation calculations which include the incoming and outgoing dividing parts of the directional couplers. It is shown that the device length can be reduced by a factor of 6 as compared to former designs.

keywords - nonreciprocal coupler, integrated optics, circulator, isolator, magneto-optic

1 Introduction

Integrated optical isolators and circulators are important components for the future development of optical communication technique. The nonreciprocal behaviour of these devices is based on the magneto-optic Faraday effect which occurs in magnetic garnet crystals. Different concepts for integrated optical isolators have been published in recent years [1, 2, 3, 4, 5, 6, 7, 8, 9]. Most of them rely on the nonreciprocal phase shift $\Delta\beta = \beta_{\mathrm{forw}} - \beta_{\mathrm{back}}$, the difference between the propagation constants of forward and backward traveling light [10]. This also offers the possibility to realize coupled waveguides with different coupling lengths for forward and backward propagation as described in [11, 12]. Such coupled waveguides can be applied as isolators and circulators, respectively if the number of couplings differs by one between the forward and backward direction. To achieve a short device length it is necessary to design coupled waveguides with a large difference in the nonreciprocal phase shifts of the symmetric and antisymmetric normal modes.

The aim of this paper is to present a new design for nonreciprocal couplers with a reduced device length compared with formerly presented coupled waveguides. The device length, including the separating parts of the directional couplers, is derived with normal mode theory. We present typical fabrication tolerances and show how the isolators can be tuned in a postfabrication process. In the last section a beam propagation method is used to simulate the circulator.

In this paper all calculations are performed for TM polarized modes. Since magneto-optic waveguides with a central compensation wall show a nonreciprocal phase shift for TE-modes [13, 14] it also possible to construct a circulator for TE-modes. The simulations referring to the TE polarization will be presented in a forthcoming paper.

2 Nonreciprocal Couplers

In this section we give a brief analysis of nonreciprocal waveguide couplers. The following calculations are performed for the basic coupler geometry sketched in Fig. 1. If the magnetization of the garnet films is adjusted in the film plane transversely to the propagation direction z the permittivity tensor is

$$\hat{\epsilon} = \begin{pmatrix} \epsilon & 0 & \mathrm{i}\xi \\ 0 & \epsilon & 0 \\ -\mathrm{i}\xi & 0 & \epsilon \end{pmatrix} \tag{1}$$

where ϵ and ξ depend on x and y. The nondiagonal element ξ represents the magneto-optic effect and is related to the specific Faraday rotation Θ_F by

$$\xi \approx 2n\Theta_\mathrm{F}/k_0, \tag{2}$$

where $n = \sqrt{\epsilon}$ is the refractive index and k_0 is the vacuum wave number.

In semi-vectorial approximation the following TM mode equation can be derived straightforwardly from

Maxwell's equations [15]

$$(-\epsilon\partial_x\epsilon^{-1}\partial_x - \partial_y^2 + \beta^2 - \epsilon\beta(\partial_x\frac{\xi}{\epsilon^2}))H_y = \epsilon k_0^2 H_y. \tag{3}$$

TE-modes are not dealt with in this paper. The term linear in β causes the nonreciprocal phase shift. Since ξ is small compared to ϵ it can be considered as a perturbation. Then perturbation theory yields

$$\Delta\beta = -\frac{\iint(\partial_x H_y)H_y(\xi/\epsilon^2)dxdy}{\iint\epsilon^{-1}|H_y|^2dxdy} \tag{4}$$

for the nonreciprocal phase shift [16].

We use a finite element method to solve for modes of the unperturbed waveguides [17]. With the calculated mode field we obtain the nonreciprocal phase shift via equation 4.

The coupling behaviour of coupled waveguides can be described either with coupled mode or normal mode theory [18, 19]. Since we deal with tightly coupled waveguides we prefer the normal mode theory. The two coupled waveguides are treated as one wide waveguide that guides in general one even and one odd mode with the propagation constants β^e and β^o (see figures 3. a) and b)). The coupling between the two waveguides can be described by the interference of the two normal modes. An input signal at one waveguide excites a superposition of the even and odd mode. After a distance L_coupling a phase difference of π between the modes has accumulated so that the power is now guided in the other waveguide. This coupling length is given by

$$L_\mathrm{coupling} = \frac{\pi}{|\beta^\mathrm{e} - \beta^\mathrm{o}|}. \tag{5}$$

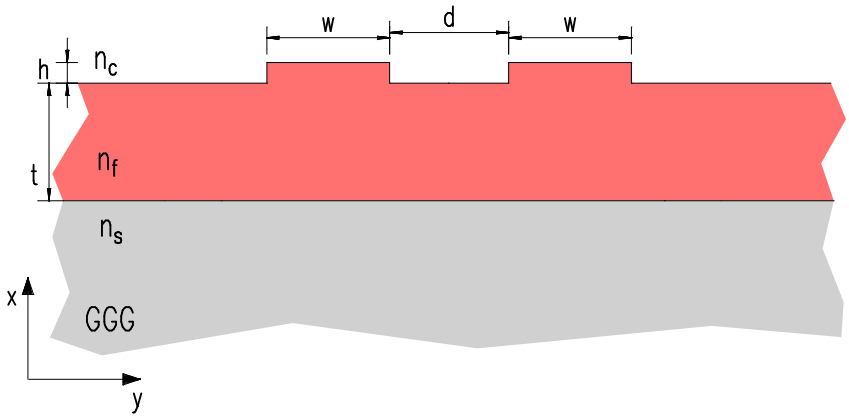

Figure 1: Basic geometry of the nonreciprocal coupled waveguides.

Equation 5 is no longer valid for z-dependent structures as sketched in figure 2. In this case the phase difference between the modes must be integrated over the propagation distance so that the power fractions at the output ports C and D (for propagation in positive z-direction) of a symmetric coupler are [20, 21]

$$P_{\mathrm{C}} = \cos^2(\phi/2) \quad \text{and} \quad P_{\mathrm{D}} = \sin^2(\phi/2) \tag{6}$$

with

$$\phi = \phi_0 + \pi \int_0^z (\beta^{\mathrm{e}}(z) - \beta^{\mathrm{o}}(z))dz. \tag{7}$$

The total power is normalized to unity and the input power at port A and B are $P_{\mathrm{A}} = \cos^2(\phi_0/2)$ and $P_{\mathrm{B}} = \sin^2(\phi_0/2)$, respectively. For the propagation in negative z-direction, (A, B) and (C, D) exchange their roles.

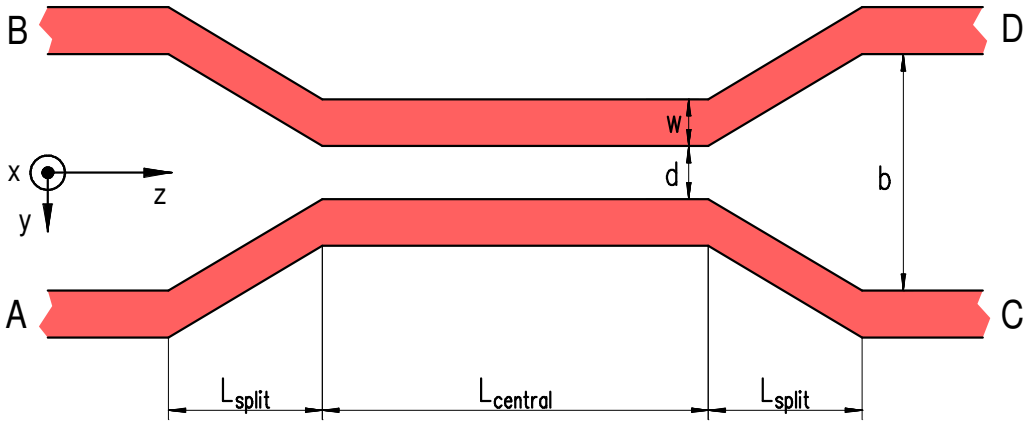

Figure 2: Schematic diagram of coupled waveguides with transition sections. The input/output ports are denoted with A to D.

Since the propagation constants $\beta^{\mathrm{e,o}}_{\mathrm{forw}}$ and $\beta^{\mathrm{e,o}}_{\mathrm{back}}$ of magneto-optic waveguides are different for forward and backward propagation (the difference is the nonreciprocal phase shift), the coupling lengths differ, too. The propagation constants are defined in the following way:

$$\beta^{\mathrm{e}}_{\mathrm{forw,back}} = \beta^{\mathrm{e}} \mp \frac{1}{2}\Delta\beta^{\mathrm{e}} \quad \text{and} \quad \beta^{\mathrm{o}}_{\mathrm{forw,back}} = \beta^{\mathrm{o}} \mp \frac{1}{2}\Delta\beta^{\mathrm{o}} \tag{8}$$

with $\Delta\beta$ given by equation 4 and where β^{e} and β^{o} are the propagation constants of the corresponding isotropic structure.

The device works as an isolator or circulator if the number of couplings in forward and backward direction differs by one. Then the input light at port A leaves the coupler at port C, while backward propagating light which enters the devices at port C leaves at port B. Likewise, port B is connected with port D in forward direction and port D is connected with port A in backward direction. For a coupler device without transition sections a suitable device length can be estimated with [12] to be

$$L_{\text{estimate}} = \frac{\pi}{|\beta^{\text{e}}_{\text{forw}} - \beta^{\text{e}}_{\text{back}} - \beta^{\text{o}}_{\text{forw}} + \beta^{\text{o}}_{\text{back}}|} = \frac{\pi}{|\Delta\beta^{\text{e}} - \Delta\beta^{\text{o}}|} \tag{9}$$

with the additional constraint that the the device length is a multiple of the coupling length. For a short device it is therefore important to have an as large as possible difference between the nonreciprocal phase shifts of the even and odd normal modes so that equation 9 can be utilized to optimize the waveguide parameters of the central coupling region.

Nevertheless, for a complete device with transition sections (see fig. 2) the output power must be calculated with equations 6 and 7 in order to derive the correct length of the central coupling section L_{central} if all other parameters are optimized before.

3 Numerical Results

For the realization of a short device we have to maximize the denominator of equation 9 $|\Delta\beta^{\text{e}} - \Delta\beta^{\text{o}}|$. Using equation 4 it can be written for normalized modes as follows

$$|\Delta\beta^{\text{e}} - \Delta\beta^{\text{o}}| = |\iint \frac{\xi}{\epsilon^2} \left[(\partial_x H^{\text{e}}_y) H^{\text{e}}_y - (\partial_x H^{\text{o}}_y) H^{\text{o}}_y\right] dxdy|, \tag{10}$$

since ξ/ϵ^2 is equal for both modes. Obviously, the term becomes maximal if the mode distributions of the even and the odd modes differ as much as possible. A further maximization is possible if ξ is positive in the regions where the difference of the $(\partial_x H_y)H_y$ terms is positive, and negative in the rest of the waveguiding film, or vice versa. In order to find these regions, we plot $(\partial_x H^{\text{e}}_y)H^{\text{e}}_y - (\partial_x H^{\text{o}}_y)H^{\text{o}}_y$ for typical coupled waveguides, (see fig. 3. c)). As one can see, the waveguide is divided into 6 nearly rectangular regions with an alternating sign of $(\partial_x H^{\text{e}}_y)H^{\text{e}}_y - (\partial_x H^{\text{o}}_y)H^{\text{o}}_y$. With this knowledge we choose a waveguide geometry, as sketched in figure 4, that minimizes the device length. The guiding magneto-optic layer is divided into 6 parts with an alternating sign of ξ, i. e. an alternating Faraday-rotation, which are bounded by magnetic compensation walls [22]. The borders should fit to the zero lines of figure 3. c) for a minimal device length.

Now we can perform a further optimization of the free waveguide parameters w, h, d, q, t_1 and t_2. The optimal film thicknesses t_1 and t_2 can be derived from simple calculations of the nonreciprocal phase shift of double layer slab waveguides since we deal with weakly etched waveguides. For typical parameters of magneto-optic waveguides ($n_{\text{s}} = 1.95$, $n_{\text{f}} = 2.30$, $n_{\text{c}} = 1$, $\xi = \pm 0.005$, i. e. $\Theta_{\text{F}} \approx \pm 3000°/\text{cm}$) $t_1 = 0.23\mu$m and $t_2 = 0.34\mu$m are best.

In order to optimize the waveguide separation d and the width q of the region with the reversed Faraday-rotation we compute L_{estimate} with equation 9 for a fixed rib width and height. The results are plotted in figure 5. Obviously, for each waveguide separation an optimal compensation wall distance q can be found that minimizes the coupler length L_{estimate}. In that case the rectangular areas with different Faraday rotation fit best to the regions with opposite sign of $(\partial_x H^{\text{e}}_y)H^{\text{e}}_y - (\partial_x H^{\text{o}}_y)H^{\text{o}}_y$, see figures 3. c) and 4. But more significant is the fact that the device length decreases steadily with a reduced waveguide

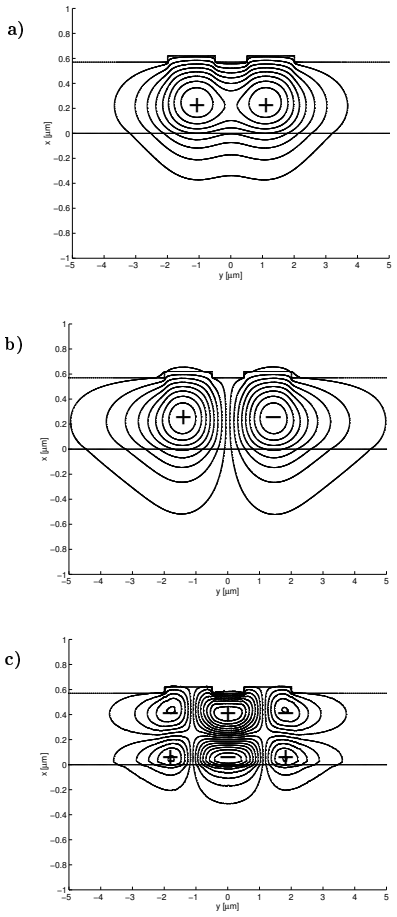

Figure 3: Calculated mode fields H_y for the even TM_0 (a)) and the odd TM_1 (b)) modes of coupled waveguides. In (c)) the difference $(\partial_x H_y^{\mathrm{e}})H_y^{\mathrm{e}} - (\partial_x H_y^{\mathrm{o}})H_y^{\mathrm{o}}$ of these two modes is shown. The modes are normalized, and + and − denote the respective sign. Parameters are: $n_{\mathrm{s}} = 1.95$, $n_{\mathrm{f}} = 2.30$, $n_{\mathrm{c}} = 1$, $w = 1.5\mu$m, $d = 1\mu$m, $t = 0.57\mu$m, $h = 0.05\mu$m and $\lambda = 1.3\mu$m.

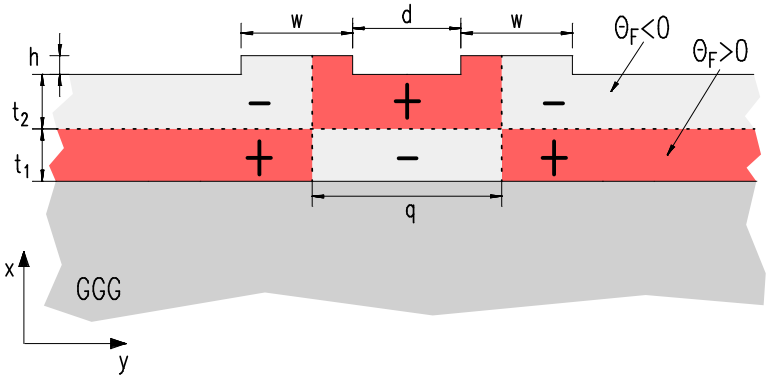

Figure 4: Schematic picture of the optimal waveguide structure for a nonreciprocal coupler. The magneto-optic regions are divided by compensation walls. In this case + and − denote the sign of the Faraday-rotation.

separation. The minimum value is found for $d = 0$. Then the coupled waveguides are degenerated to one broad rib. The reason for this behaviour is self-evident. In the gap region we observe a stricture of the even TM-mode, (see fig. 3. a)), which disappears if we take only one wide rib. Then the difference in the mode profiles of the even and the odd

TM-modes becomes maximal, and this leads to a minimal length L_{estimate}.

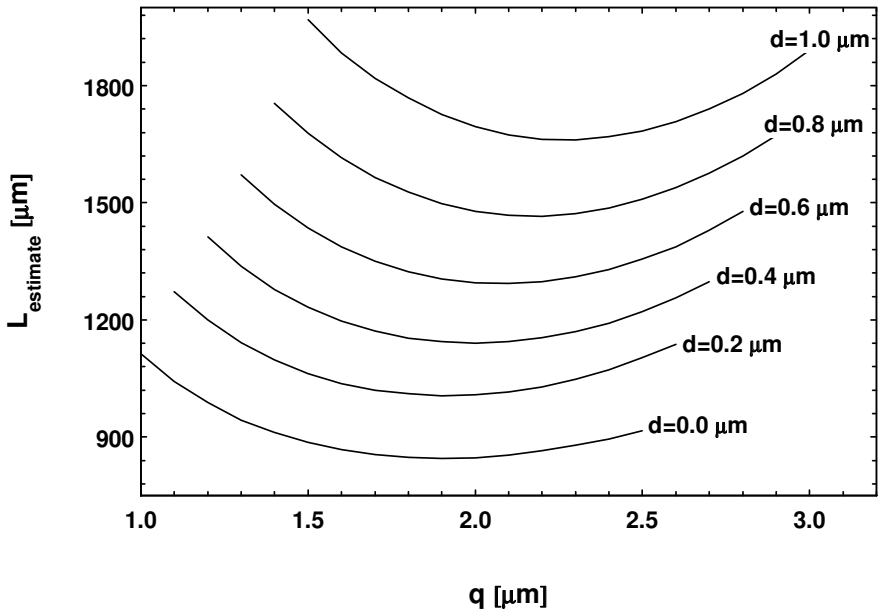

Figure 5: Computed minimal length L_{estimate} of the nonreciprocal coupler for a rib width of $w = 1.5\mu$m and an etch depth of $h = 0.05\mu$m. The other waveguide parameters are given in the text.

So far we have not regarded the influence of the rib geometry. Therefore, we compute the coupler length L_{estimate} for different rib widths versus the compensation wall separation q. The rib height h is 0.05μm, and the waveguide distance is now zero. As can be seen in figure 6, the minimal coupler length decreases with the rib width. The same effect occurs for the rib height which is not shown here. The reason for this effect is that the odd TM-mode of the waveguide approaches cut-off with a decreasing rib height or width. As the expansion of the odd mode increases strongly in the region near to cut-off, the differences in the mode field distributions grow. This leads to a reduced coupler length. The problem with this situation is that it is always critical to operate a device in the region of the mode cut-off. It seems to be a good compromise to use the following waveguide geometry in the central part of the directional coupler for further simulation: $w = 1.5\mu$m, that means a total rib width of 3.0μm, $h = 0.05\mu$m and $q = 2.0\mu$m. The computation with these parameters leads to $\Delta\beta^{\text{e}} = 17.9\text{cm}^{-1}$, $\Delta\beta^{\text{o}} = -19.2\text{cm}^{-1}$, and $L_{\text{estimate}} = 846\mu$m. Note the different signs of the nonreciprocal phase shifts of the even and odd modes due to the alternating sign of the Faraday rotation in the central part of the waveguide.

For a simpler realization of the devices it may be also attractive to consider a geometry where the central or the outer magneto-optic double layer is replaced by a dielectric material of equal refractive index. In these cases the coupler length is doubled.

Now we can start to model the entire device, including the splitting regions on both sides of the main coupling part. These transition sections are essential for the connection of the circulator with other integrated optical devices. The spacing of the waveguides at the input and output, respectively, must be large enough so that a mutual influence of the waveguides is negligible. Furthermore, the sections should be so long that a smooth transfer of the power to the central waveguide coupler is warranted. For further simulations we assume a maximal waveguide separation of $b = 8\mu$m and a splitter length of $L_{\text{split}} = 400\mu$m. See figure 2 for the definitions of b and L_{split}.

In order to find the optimal length of the main coupling section L_{central}, we derive the

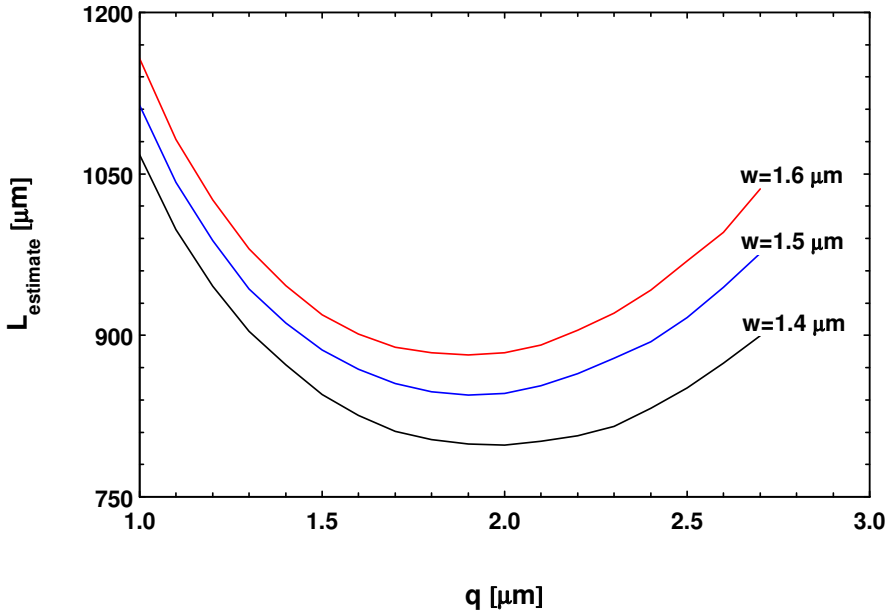

Figure 6: Computed length L_{estimate} of the nonreciprocal coupler for different rib widths. The etch depth is $h = 0.05\mu$m and $d = 0\mu$m. The other waveguide parameters are given in the text.

output power at port C and D for the forward direction ($P_{\text{A}\to\text{C}}$, $P_{\text{A}\to\text{D}}$, $P_{\text{B}\to\text{C}}$, $P_{\text{B}\to\text{D}}$) using equations 6 to 8 with the given parameters. The power input is assumed to be at ports A and B, respectively. For the backward direction we calculate the output power at ports A and B ($P_{\text{C}\to\text{A}}$, $P_{\text{C}\to\text{B}}$, $P_{\text{D}\to\text{A}}$, $P_{\text{D}\to\text{B}}$). In this case we define ports C and D as input channels.

If the devices should work as circulators $P_{\text{A}\to\text{C}}$ must be unity and $P_{\text{C}\to\text{A}}$ must be zero for the straight connection (A↔C). For the diagonal connection (C↔B) $P_{\text{C}\to\text{B}}$ should be unity and $P_{\text{B}\to\text{C}}$ should be zero for the optimal length L_{central}. Due to the symmetry of the couplers the requirements for the remaining connections (B↔D) and (D↔B) then are automatically fulfilled. For a better presentation we plot only $P_{\text{A}\to\text{C}}$ and $P_{\text{C}\to\text{B}}$ versus the length L_{central}. For a circulator, both should be unity at the same length of the main coupling part. The results in figure 7 show the sinusoidal behaviour of $P_{\text{A}\to\text{C}}$ and $P_{\text{C}\to\text{B}}$. Due to the different period, they are almost in phase only for coupler lengths from 700μm up to 800μm. One obtains an circulator for $L_{\text{central}} = 760\mu$m as indicated by the inset. Obviously, the used parameters are not yet optimal since $P_{\text{A}\to\text{C}}$ and $P_{\text{C}\to\text{B}}$ have not exactly the same phase at the maximum so that the isolation ratio is limited at the outset. For our set of parameters the maximal achievable isolation degree is 28.8dB if the isolation is defined as the minimum isolation for the straight and diagonal connection, respectively:

$$\text{Isolation[dB]} = \min\{10\log_{10}(P_{\text{A}\to\text{C}}/P_{\text{C}\to\text{A}}),\ 10\log_{10}(P_{\text{C}\to\text{B}}/P_{\text{B}\to\text{C}})\}. \qquad (11)$$

This problem can be solved if the compensation wall separation q is shifted a little. This has no influence on the unperturbed modes, only the nonreciprocal phase shift is changed. Therefore, we can shift the point where $P_{\text{A}\to\text{C}}$ and $P_{\text{C}\to\text{B}}$ are in phase. The arrows in figure 8 indicate the points where both curves are in phase for growing q. As one can see, the point moves over the local maximum. An isolation larger than 40dB is achieved for $q = 2.29\mu$m if we choose $L_{\text{central}} = 759\mu$m. The result is a total device length of 1559μm which is more than 6 times shorter than a formerly presented design [12].

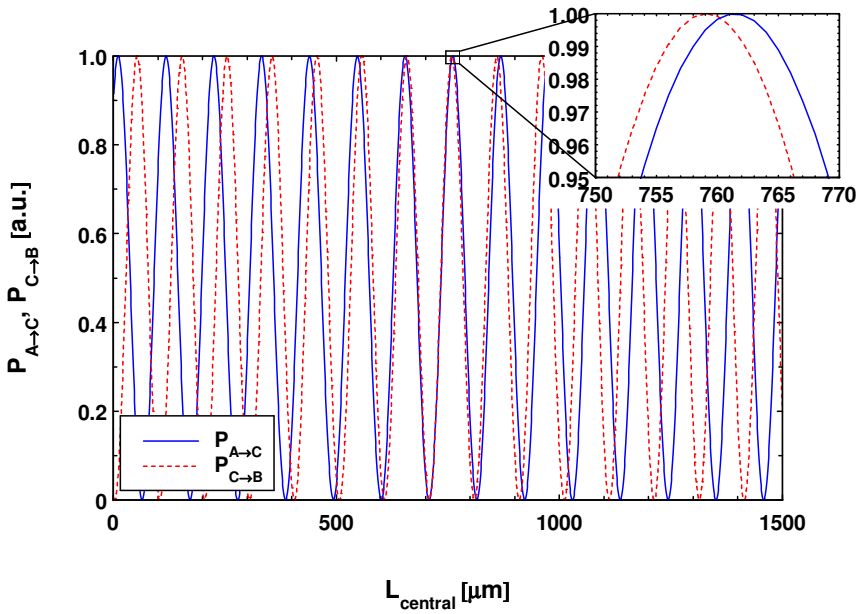

Figure 7: The output power $P_{\mathrm{A}\to\mathrm{C}}$ and $P_{\mathrm{C}\to\mathrm{B}}$ for the nonreciprocal coupler of fig. 2 versus the length L_{central}. Parameters are: $n_{\mathrm{s}} = 1.95$, $n_{\mathrm{f}} = 2.30$, $n_{\mathrm{c}} = 1$, $w = 1.5\mu$m, $d = 0\mu$m, $q = 2.0\mu$m, $t_1 = 0.23\mu$m, $t_2 = 0.34\mu$m, $h = 0.05\mu$m, $\xi = \pm 0.005\mu$m, $b = 8\mu$m, $L_{\mathrm{split}} = 400\mu$m and $\lambda = 1.3\mu$m.

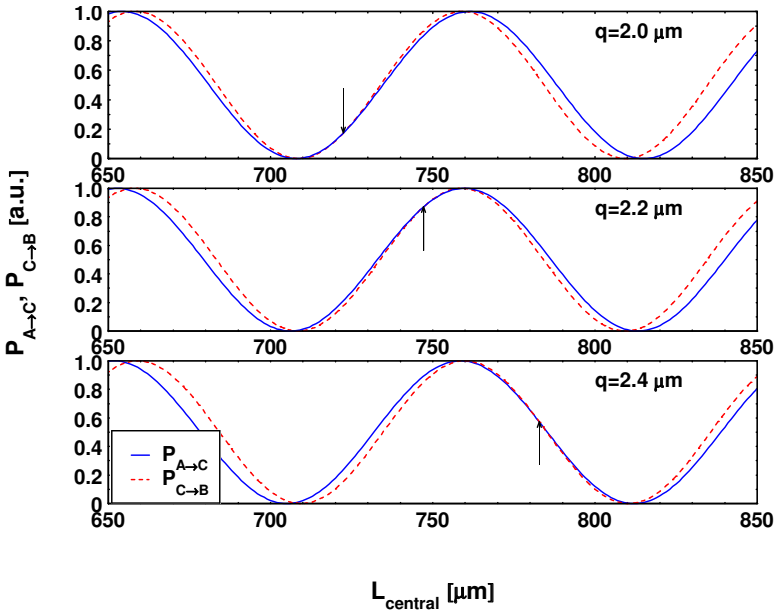

Figure 8: The output power $P_{\mathrm{A}\to\mathrm{C}}$ and $P_{\mathrm{C}\to\mathrm{B}}$ for the nonreciprocal coupler of fig. 2 versus the length L_{central} for different distances of the vertical compensation wall q. The parameters are the same as in fig. 7.

4 Fabrication Tolerances

For future fabrication of the circulator it is important to know how the variation of the device parameters influence the performance. Therefore, we calculate the isolation ratio for the variation of one parameter in the range of typical fabrication tolerances. The results are presented in table 1. It is evident, that the parameters which influence only the nonreciprocal effect, like q and ξ, reduce the isolation only slightly, whereas the deviation

Isolation [dB]	j						
	-3	-2	-1	0	+1	+2	+3
$2w$=3.00μm+j·0.005μm	21.67	23.50	29.02	>40	28.69	23.21	19.40
h=0.05μm+j·0.0002μm	14.70	18.12	23.36	>40	26.34	19.57	15.30
L_{central}=759μm +j·1μm	20.03	23.31	28.54	>40	31.97	24.98	21.14
q=2.29μm+j·0.01μm	26.17	29.31	29.00	>40	31.93	22.29	20.14
t_1=0.34μm+j·0.0004μm	25.04	28.69	35.56	>40	30.51	25.83	22.83
t_2=0.23μm+j·0.0004μm	25.17	29.42	35.60	>40	29.97	26.23	23.41
λ=1.30μm+j·0.005μm	19.64	22.94	28.13	>40	32.59	25.66	21.85
ξ=0.005 +j·0.0001	26.61	29.59	34.18	>40	33.29	29.06	26.23
n_{f}=2.30 +j·0.002	16.99	20.35	25.74	>40	29.02	22.25	18.48

Table 1: Computed isolation of the nonreciprocal coupler for different deviations of the waveguide parameters from optimal values.

of the film thicknesses t_1 and t_2 and especially of the rib height h from the ideal values lead to a strong decrease of the performance. Although the rib height can be controlled by ion beam etching very precisely, it seems to be impossible to achieve a reproducible isolation of at least 30dB.

Because of this reason, we propose the following tuning procedure. The film thickness t_2 can be reduced after the fabrication of the nonreciprocal coupler. This has the effect that the maximal isolation is always shifted to shorter lengths of the central coupling section, as plotted in figure 9. Therefore, the coupler can be produced in a first step some microns shorter than calculated with the optimal waveguide parameters. Then it is possible to shift the maximal isolation to the given length by a stepwise reduction of the film thickness.

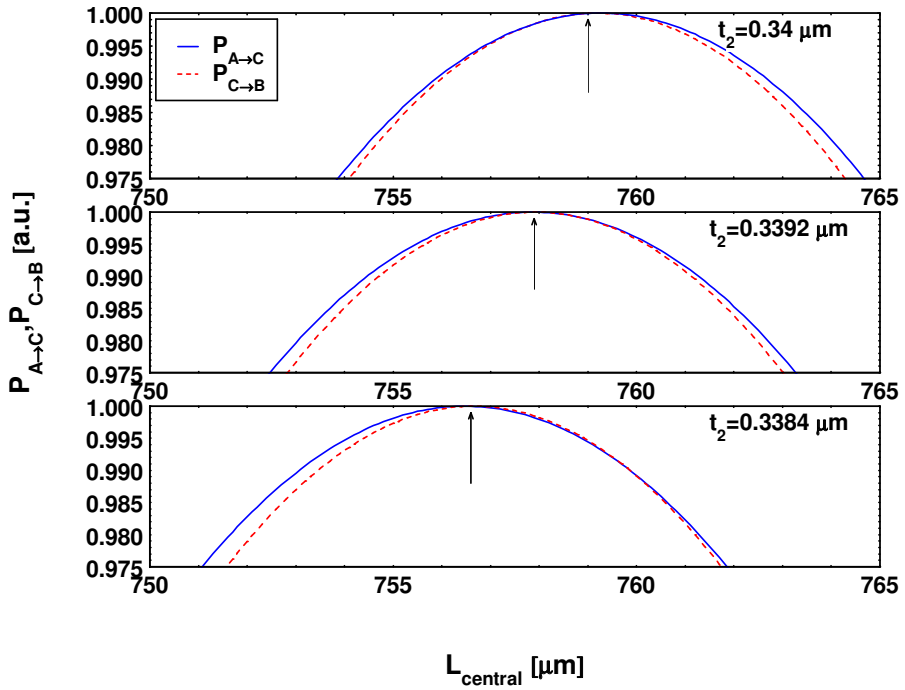

Figure 9: The output power $P_{\mathrm{A}\to\mathrm{C}}$ and $P_{\mathrm{C}\to\mathrm{B}}$ for the nonreciprocal coupler versus the length L_{central} for different film thicknesses t_2. The arrows indicate the lengths with maximal isolation. The parameters are the same as in fig. 7, and $q = 2.29\mu$m.

5 Beam Propagation Method

Another method to simulate the behaviour of the proposed circulators is a finite difference beam propagation method (BPM). Different beam propagation techniques were implemented by various groups [23, 24, 25]. First BPM calculations of planar magneto-optic slab waveguides were performed in [26]. A BPM for magneto-optic rib-waveguides was first used to simulate light propagation in a nonreciprocal Mach-Zehnder interferometer [9].

We use the same method again to compute the nonreciprocal light propagation in the directional couplers. For this purpose we divide the cross-section of the coupler in 7 slab waveguides and calculate effective refractive indices n_{eff} for the regions. Since the refractive indices differ for the forward and backward direction, the BPM calculations must be performed for each direction separately.

From Maxwell's equation one obtains in paraxial approximation the following Fresnel equation [24]

$$2\mathrm{i}k_0 n_{\text{ref}} \frac{\partial E_x}{\partial z} = \frac{\partial^2 E_x}{\partial y^2} + k_0^2[n_{\text{eff}}^2(y) - n_{\text{ref}}^2]E_x \tag{12}$$

for the E_x component of the electric field. This is the dominating electric field component of the TM-mode. We take the mean value of the even and odd normal mode in the central section for the reference index n_{ref}. The Fresnel equation is solved with a finite difference Crank-Nicolson algorithm. Transparent boundary conditions suppress reflections at the boundary [27].

In order to find the optimal length of the central coupling region L_{central} we perform several runs of the BPM for different coupler lengths and calculate the output power for forward and backward directions. The total output power is always normalized to 1. Results are shown in figure 10. For $L_{\text{central}} = 782\mu$m we find the optimal isolation. Due to the effective index approximation this length differs from the results which are obtained by the normal mode calculations. Otherwise the results have a comparable behaviour.

The BPM simulation for $L_{\text{central}} = 782\mu$m is depicted in figure 11. The left part shows the light propagation in forward direction while the intensity of backward propagating light is plotted in the right part. The parameters are chosen to be the same as in fig. 7, $q = 2.29\mu$m. In forward direction the power is coupled 16 times from one to the other side, while there are 17 couplings in backward direction. Therefore, the device performs as a circulator.

6 Summary

In this paper we perform a rigorous normal mode simulation of nonreciprocal directional couplers, including the X-like transition sections. The proposed coupler geometry with different double layer magneto-optic films with an alternating sign of the Faraday-rotation reduces the total device length by a factor 6 as compared to formerly presented couplers. It is shown that it is possible to achieve simultaneously an isolation larger than 40 dB for the straight and diagonal connection of the circulator. Because fabrication tolerances are rather critical, a postfabrication tuning is necessary. Simple BPM calculations are used to show the operation of the circulator.

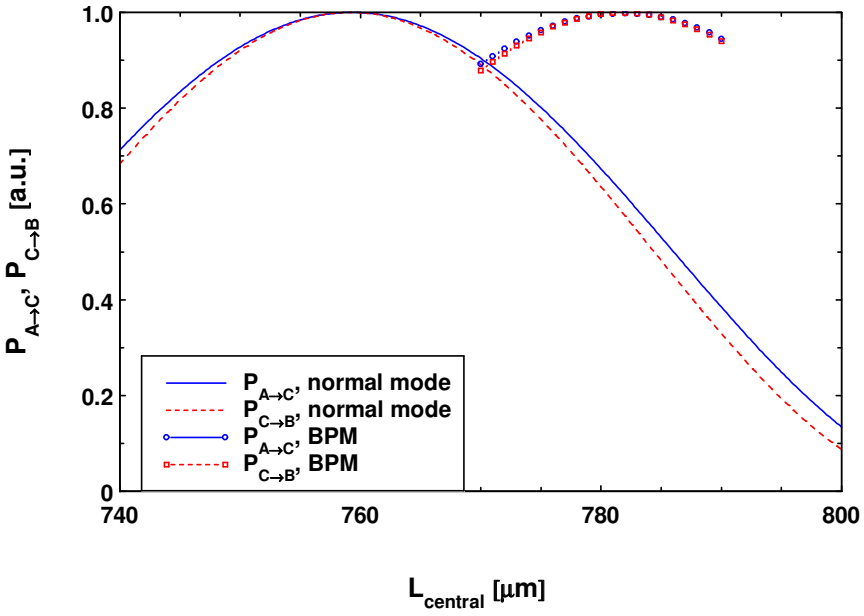

Figure 10: Computed output power of the nonreciprocal coupler versus the length L_{central} with the BPM and normal mode method. The parameters are the same as in fig. 7, and $q = 2.29\mu$m.

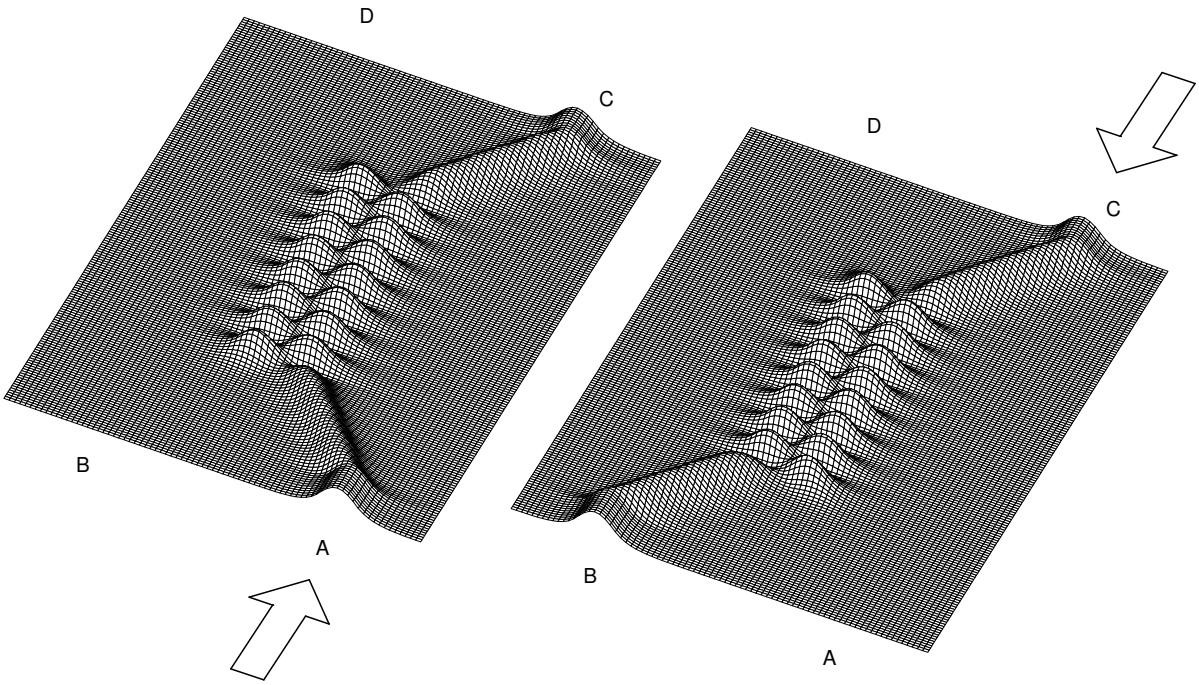

Figure 11: BPM simulation of the light propagation in the nonreciprocal coupler. The parameters are the same as in fig. 7, $q = 2.29\mu$m, and $L_{\text{central}} = 782\mu$m. Note the different scales in longitudinal and lateral directions.

Acknowledgements

We gratefully acknowledge financial support by Deutsche Forschungsgemeinschaft, Sonderforschungsbereich 225.

References

[1] R. Wolfe, J.F. Dillon Jr., R. A. Lieberman, and V. J. Fratello, "Broadband magneto-optic waveguide isolator," *Applied Physics Letters*, vol. 57, no. 10, pp. 960, 1990.

[2] K. Ando, T. Okoshi, and N. Koshizuka, "Waveguide magneto-optic isolator fabricated by laser annealing," *Applied Physics Letters*, vol. 53, no. 1, pp. 4–6, 1988.

[3] T. Mizumoto, Y. Kawaoka, and Y. Naito, "Waveguide-Tpye Optical Isolator Using the Faraday and the Cotton-Mouton Effects," *The Transactions of the IECE of Japan*, vol. E 69, no. 9, pp. 968–972, 1986.

[4] H. Hemme, H. Dötsch, and P. Hertel, "Integrated optical isolator based on nonreciprocal-mode cut-off," *Applied Optics*, vol. 29, no. 18, pp. 2741–2744, 1990.

[5] S. Yamamoto, Y. Okamura, and T. Makimoto, "Analysis and Design of Semileaky-Type Thin-Film Optical Waveguide Isolator," *IEEE Journal of Quantum Electronics*, vol. QE-12, no. 12, pp. 764–770, 1976.

[6] T. Shintaku, "Integrated optical isolator based on nonreciprocal higher-order mode conversion," *Applied Physics Letters*, vol. 66, no. 21, pp. 2789–2791, 1995.

[7] F. Auracher and H.H. Witte, "A new design for an integrated optical isolator," *Optics Communications*, vol. 13, no. 4, pp. 435–438, 1975.

[8] Y. Okamura, T. Negami, and S. Yamamoto, "Integrated optical isolator and circulator using nonreciprocal phase shifters: a proposal," *Applied Optics*, vol. 23, no. 11, pp. 1886–1889, 1984.

[9] N. Bahlmann, M. Lohmeyer, M. Wallenhorst, H. Dötsch, and P. Hertel, "An improved design of an integrated optical isolator based on nonreciprocal Mach-Zehnder interferometry," *Optical and Quantum Electronincs*, vol. 30, no. 5/6, pp. 323–334, 1998.

[10] S. Yamamoto and T. Makimoto, "Circuit theory for a class of anisotropic and gyrotropic thin-film optical waveguides and design of nonreciprocal devices for integrated optics," *Journal of Applied Optics*, vol. 45, no. 2, pp. 882–888, 1974.

[11] T. Mizumoto, O. Kiyoshi, T. Harada, and Y. Naito, "Measurement of Optical Nonreciprocal Phase Shift in a Bi-Substituted $Gd_3Fe_5O_{12}$ Film and Application to Waveguide-Type Optical Circulator," *Journal of Lightwave Technology*, vol. LT-4, no. 3, pp. 347–352, 1986.

[12] A. Erdmann, P. Hertel, and H. Dötsch, "Nonreciprocal coupling effects in gyrotropic waveguide structures," *Optical and Quantum Electronics*, vol. 26, pp. 949–955, 1994.

[13] A. F. Popkov, M. Fehndrich, M. Lohmeyer, and H. Dötsch, "Nonreciprocal TE-mode phase shift by domain walls in magnetooptic rib waveguides," *Applied Physics Letters*, vol. 72, no. 20, pp. 2508–2510, 1998.

[14] N. Bahlmann, M. Lohmeyer, H. Dötsch, and P. Hertel, "Finite element analysis of nonreciprocal phase shift for TE-modes in magneto-optic rib-waveguides with a compensation wall," *IEEE Journal of Quantum Electronics*, vol. 0, no. 0, pp. 0–0, 1998.

[15] A. Erdmann, M. Shamonin, P. Hertel, and H. Dötsch, "Finite difference analysis of gyrotropic waveguides," *Optics Communications*, vol. 102, no. 1,2, pp. 25–30, 1993.

[16] M. Shamonin and P. Hertel, "Analysis of nonreciprocal mode propagation in magneto-optic rib-waveguide structures with the spectral-index method," *Applied Optics*, vol. 33, no. 27, pp. 6415–6421, 1994.

[17] M. Koshiba and X.P. Zhuang, "An Efficient Finite-Element Analysis of Magnetooptic Channel Waveguides," *Journal of Lightwave Technology*, vol. 11, no. 9, pp. 1453–1458, 1993.

[18] E. Marom, O. G. Ramer, and S. Rushin, "Relation Between Normal-Mode and Coupled-Mode Analysis of Parallel Waveguides," *IEEE Journal of Quantum Electronics*, vol. QE-20, no. 12, pp. 1311–1319, 1984.

[19] D. G. Hall and B. J. Thompson, Eds., *Selected Papers on Coupled-Mode Theory in Guided-Wave Optics*, SPIE Milestone Series. SPIE Optical Engineering Press, Bellingham, Washington USA, 1993.

[20] C. Vasallo, "About Coupled-Mode Theories for Dielectric Waveguides," *Journal of Lightwave Technology*, vol. 6, no. 2, pp. 294–303, 1988.

[21] W. Karthe and R. Müller, *Integrierte Optik*, Akademische Verlagsgesellschaft Geest & Portig, Leipzig, 1991.

[22] R. Wolfe, J. Hegarty, J.F. Dillon Jr., L.C. Luther, G.K. Celler, and L.E. Trimble, "Thin-film waveguide magneto-optic isolator," *Applied Physics Letters*, vol. 46, no. 9, pp. 817–819, 1985.

[23] M. D. Feit and J. A. Fleck Jr., "Light propagation in graded-index optical fibers," *Applied Optics*, vol. 17, no. 24, pp. 3990–3998, 1978.

[24] Y. Chung and N. Dagli, "An Assessment of Finite Difference Beam Propagation Method," *IEEE Journal of Quantum Electronics*, vol. 26, no. 8, pp. 1335–1339, 1990.

[25] H. J. W. M. Hoekstra, "On beam propagation methods for modelling in integrated optics," *Optical and Quantum Electronics*, vol. 29, pp. 157–171, 1997.

[26] A. Erdmann and P. Hertel, "Beam-Propagation in Magnetooptic Waveguides," *IEEE Journal of Quantum Electronics*, vol. 31, no. 8, pp. 1510–1516, 1995.

[27] G. R. Hadley, "Transparent boundary condition for beam propagation," *Optics Letters*, vol. 16, no. 9, pp. 624–626, 1991.